Computer Simulation and Visualization of Mechanical Wave Propagation Phenomena in Continuous Medium

Rodrigo Mologni G. dos Santos José Mario De Martino Euclides de Mesquita Neto

DCA, FEEC, Unicamp
Av. Albert Einstein, 400
Cidade Universitária
13083-852, Campinas, SP, Brazil

DMC, FEM, Unicamp
R. Mendeleyev, 200
Cidade Universitária
13083-860, Campinas, SP, Brazil

mologni@dca.fee.unicamp.br martino@dca.fee.unicamp.br euclides@fem.unicamp.br

ABSTRACT

This paper presents a simulation software for mechanical wave propagation phenomena and a visualization environment developed to help the analysis of the numerically synthesized dynamic solutions of boundary value problems of solid mechanics. The simulation software is used by researchers and engineers to study and gain insights into complex problems related to the mechanics of continuous media. The large amount of data generated by the numerical solution of wave propagation problems makes the interpretation of the results a hard daunting task without the support of techniques to graphically display these data. The visualization environment that was developed supports different visualization strategies of a variety of parameters and it has been used to improve the understanding of the simulation results and to validate the numerical simulator as well as the underlying mathematical-physical modeling.

Keywords

Computer simulation, scientific visualization, mechanical waves.

1. INTRODUCTION

The study of the mechanical wave propagation phenomena and their consequences usually requires computational methods for the resolution of complex problems in mechanics of continuous media, such as finite and boundary element methods. These computational methods consist of mathematical modeling and computer simulation of physical problems, which replace in many cases the use of costly prototypes and laboratory setups. However, the computer simulation produces a large amount of numerical data that makes the procedure of the analysis of the results an arduous and extremely difficult task without the support of data visualization techniques. With the support of visualization, researchers and engineers can more quickly validate the processes of mathematical modeling and computer simulation of the physical problems; and also they can more easily understand the results generated in the process of computer simulation, which allows a more efficiently study of the physical problems.

2. RELATED WORKS

The present work is concentrated on wave propagation in solid continua, particularly in unbounded domains. The problems to be solved are very complex and solution can only be accomplished by resorting to numerical methods. The numerical solution for two-dimensional wave problems can be found, exemplarily, in the works of Rajapakse and Wang [Raj93] and Barros et al. [Bar99]. More recently three-dimensional problems have been solved by Mesquita and his co-workers [Mes09].

3. MATHEMATICAL MODELING AND COMPUTER SIMULATION

To illustrate the features of the simulation software a complex wave propagation problem will be numerically solved. The problem solution, that is, the displacement components of the wave field solution will be analyzed and interpreted with the aid of the visualization environment. The problem at hand can be depicted at Fig. 1. It represents a series of 50 horizontal transversely isotropic (visco)elastic layers excited harmonically by a surface stress distribution

$t_z(x,\ z=0)$. The problem has a stationary character and the analysis is performed in the frequency domain. The layers are supported by a transversely isotropic half-space.

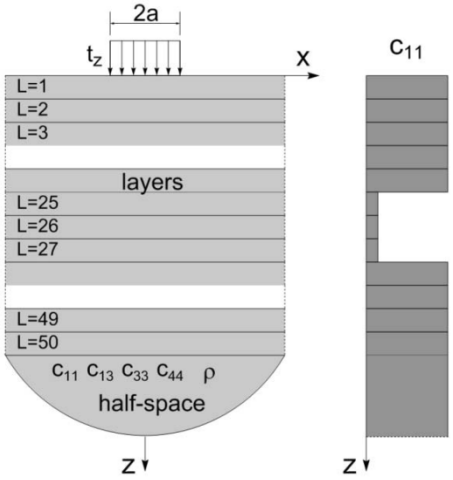

Figure 1. The geomechanical problems: horizontal layers on a half-space

Every layer is governed by a set of differential equations, which can be expressed in terms of the horizontal u_x and vertical u_z displacement components as:

$$c_{11}u_{x,xx}+c_{44}u_{x,zz}+\left(c_{13}+c_{44}\right)u_{z,xz}+\rho\omega^2u_x=0$$
$$c_{44}u_{z,xx}+c_{33}u_{z,zz}+\left(c_{13}+c_{44}\right)u_{x,xz}+\rho\omega^2u_z=0 \quad (1)$$

In Eq. 1, c_{ij} $(ij=11,\ 13,\ 33,\ 44)$ and ρ are constitutive parameters of the elastic layer [Bar99]. The circular frequency is designated by ω. The prescribed boundary conditions are the stress free surface outside the loaded area $(-a<x<a,\ z=0)$ and the Sommerfeld radiation condition at the layers and at the underlying half-space.

As can be seen in Fig. 1, the constitutive parameters of all the layers and of the half-space are the same, except for layers 25 to 27, in which there is an abrupt change in this parameters. Fig. 1 also shows the variation of the constitutive parameter c_{11} throughout the layers. This parameter discontinuity generates a strong impedance change with significant influence on the wave propagation pattern, as will be discussed later on this article.

A typical numerical expression for the harmonic wave displacement solution is given by [Bar99]:

$$u_x(x,z)=\frac{\delta}{\sqrt{2\pi}}\int_{-\infty}^{\infty}\sum_{m=1}^{2}\left(\bar{\omega}(\xi_m)A_me^{-\delta\xi_mz}-\bar{\omega}(\xi_m)B_me^{\delta\xi_mz}\right)e^{i\delta\zeta x}d\zeta$$
$$u_z(x,z)=\frac{\delta}{\sqrt{2\pi}}\int_{-\infty}^{\infty}\sum_{m=1}^{2}\left(A_me^{-\delta\xi_mz}+B_me^{\delta\xi_mz}\right)e^{i\delta\zeta x}d\zeta \quad (2)$$

4. COMPUTER VISUALIZATION

To help the analysis and understanding of the simulation results, the simulated data are enriched with additional application domain specific information.

Displacement and relative position

Propagation of mechanical waves causes the particles of matter to oscillate around their resting position. In simulation results, these oscillations are generated by action of the displacement components. Thus the displacement of an oscillating particle from its equilibrium position at time instant (t) is given by planar vector:

$$\vec{d}_t=\left(\vec{d}_{x,t},\vec{d}_{z,t}\right)\Rightarrow\begin{cases}\vec{d}_{x,t}=\mathrm{Re}(u_x)\cos t-\mathrm{Im}(u_x)\sin t\\ \vec{d}_{z,t}=\mathrm{Re}(u_z)\cos t-\mathrm{Im}(u_z)\sin t\end{cases} \quad (3)$$

Where Re and Im stand for the real and imaginary parts of a complex number, respectively.

The relative position of an oscillating particle, i.e., its new position after displacement, is given by $P_t=P+\vec{d}_t=(x_t,\ z_t)$. Where $P=(x,\ z)$ is the resting or equilibrium position and $\{t\in\mathbb{R}\mid 0\le t<2\pi\}$.

Displacement trajectory

When the oscillating particle movement is composed by overlapping simple harmonic motions of same frequency in both coordinate axes, then its oscillation describes an elliptical trajectory. As an ellipse can be drawn from its vertices, then the displacement trajectory of an oscillating particle can be represented by an ellipse whose vertices are the relative positions P_{t_k} to $k=\{1,\ 2,\ 3,\ 4\}$, where t_k is:

$$t_k=\frac{\tan^{-1}\left\{\dfrac{2\left[\mathrm{Re}(u_x)\,\mathrm{Im}(u_x)+\mathrm{Re}(u_z)\,\mathrm{Im}(u_z)\right]}{\mathrm{Im}(u_x)^2-\mathrm{Re}(u_x)^2+\mathrm{Im}(u_z)^2-\mathrm{Re}(u_z)^2}\right\}+(k-1)\pi}{2} \quad (4)$$

Aspect ratio

Since the displacement trajectory is elliptical, then the characteristics of an ellipse can also be used to enrich the simulation results. One is the aspect ratio, that is, the ratio (b/a) of the semi-major (a) and semi-minor (b) axes of an ellipse, where:

$$a=\begin{cases}\left\|\vec{d}_{t_1}\right\|,\ \left\|\vec{d}_{t_1}\right\|>\left\|\vec{d}_{t_2}\right\|\\ \left\|\vec{d}_{t_2}\right\|,\ \left\|\vec{d}_{t_1}\right\|<\left\|\vec{d}_{t_2}\right\|\end{cases},\quad b=\begin{cases}\left\|\vec{d}_{t_1}\right\|,\ \left\|\vec{d}_{t_1}\right\|<\left\|\vec{d}_{t_2}\right\|\\ \left\|\vec{d}_{t_2}\right\|,\ \left\|\vec{d}_{t_1}\right\|>\left\|\vec{d}_{t_2}\right\|\end{cases} \quad (5)$$

Rotational movement sense

The rotational movement sense (R) of the elliptical trajectory of oscillating particles can be obtained by vector dot product between the normal vectors to the planes of the trajectories $(\vec{d}_{t_1}\times\vec{d}_{t_2})$ and the medium

($\vec{n}$); see Eq. 6. Thus, if result is negative, then R is clockwise (CW); otherwise, if result is positive, then R is counter-clockwise (CCW).

$$R = \begin{cases} CW, & \vec{d}_{t_1} \times \vec{d}_{t_2} \cdot \vec{n} < 0 \\ CCW, & \vec{d}_{t_1} \times \vec{d}_{t_2} \cdot \vec{n} > 0 \end{cases} \tag{6}$$

Phase angle

The phase angle of the waves on each oscillating particle in the z-axis coordinate is given by:

$$\phi_z = \tan^{-1}\left[\frac{\mathrm{Im}(u_z)}{\mathrm{Re}(u_z)}\right], \quad -\pi \le \phi_z \le \pi \tag{7}$$

5. RESULTS AND DISCUSSION

To illustrate the power and usefulness of the visualization strategy adopted, the numerical solution of the problem described in Section 3 is used as a case study. The problem is a two-dimensional, plain strain solution [Lai09], determined at the (x, z) plane. For the calculated solution the parameters are: $a = 1m$, $\omega = 1\,rad/s$, $\rho = 1\,kg/m^3$, $t_z = 1N$, $c_{11} = 6\,N/m^2$, $c_{13} = 4\,N/m^2$, $c_{33} = 6\,N/m^2$, and $c_{44} = 1\,N/m^2$ for all the layers and the half-space, except for layers 25 to 27 in which c_{11}, c_{13}, c_{33}, and c_{44} are reduced to 10%. The data are generated on a uniform rectilinear grid composed of 5,151 (101 x 51) sampling points.

Visualization of the displacement

Fig. 2 depicts the vertical component of the displacement field (x, z, u_z) within the solution range of the problem. The location $(-a < x < a, z = 0)$ of the applied vertical excitation t_z and the "fault", that is the discontinuity in the constitutive parameters of layers 25 to 27, can be clearly recognized. Another issue that can be observed in these components is that there is no wave reflection at the end of calculation domains. On the other hand, the impedance discontinuity at layers 25 to 27 clearly causes wave transmission and reflection, distorting the wave pattern relative to the homogeneous domain.

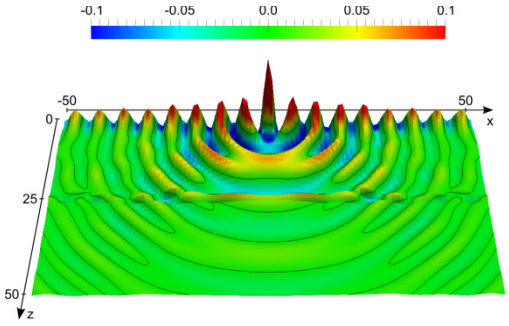

Figure 2. u_z vertical component at time $0.19 \cdot 2\pi$

Visualization of the aspect ratio

In homogeneous solids there are two broad classes of linear waves. The body waves and the surface or interface waves [Gra91]. Body waves such as the dilatational and shear waves present a rather rectilinear trajectory and they tend to cross a 2D homogeneous medium in a circular pattern, starting from the perturbation source. Surface waves such as the Rayleigh waves tend to have retrograde elliptical trajectories and are limited to the surroundings of surfaces. Fig. 3 shows an overview of the particle trajectory aspect ratio. Depending on the constitutive parameters of the medium, the values for the aspect ratio around 0.6 to 0.7 indicate the presence of Rayleigh waves [Gra91]. In Fig. 3, the elliptical Rayleigh wave trajectories are characterized by the color range going from green to yellow, as indicated in the scale (see black isolines).

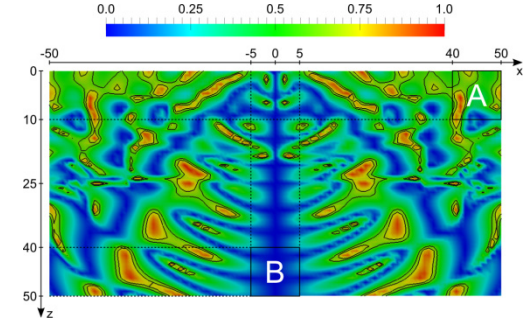

Figure 3. Aspect ratio of the elliptical trajectories

Visualization of the displacement trajectory

At the free surface $(x, z = 0)$, as the analysis moves away from the energy source, the trajectories became elliptical and decrease very rapidly, as can be seen in Fig. 4a, depicting the trajectories within the range $(40 \le x \le 50,\ 0 \le z \le 10)$. These rapidly decaying elliptical trajectories indicate the presence of Rayleigh waves. The trajectories at the range $(-5 \le x \le 5,\ 40 \le z \le 50)$ are shown in Fig. 4b. The trajectories show a predominance of body waves, characterized by the almost-rectilinear character of the displacements. As the distance from the surfaces or interfaces increases, the body forces tend to dominate the propagation pattern.

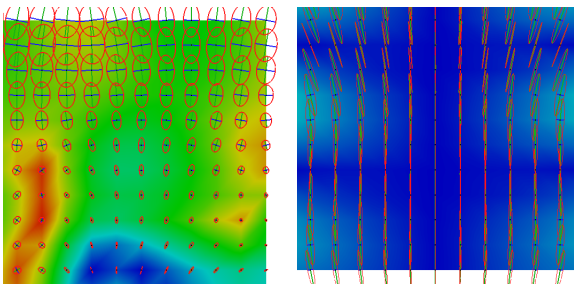

(a) Region A in Fig. 3 (b) Region B in Fig. 3

Figure 4. Displacement trajectories

Visualization of the rotational movement sense

The Rayleigh surface waves present a retrograde elliptical trajectory, as already described. Fig. 5 indicates the rotation sense of the particle trajectories. It can be clockwise (blue) or counter-clockwise (red). Now the trajectories along near the surface ($z = 0$) in the positive x-direction ($x > a$) are considered. Joining the information of Fig. 3, which states that aspect ratio of the elliptical trajectory near the surface has a value around 0.65, with the information of Fig. 4a, showing the elliptical character of the trajectory, and information of Fig. 5, stating the particle rotation sense is counter-clockwise, it may be established with a fair amount of confidence that the waves propagating at this region are predominantly Rayleigh waves.

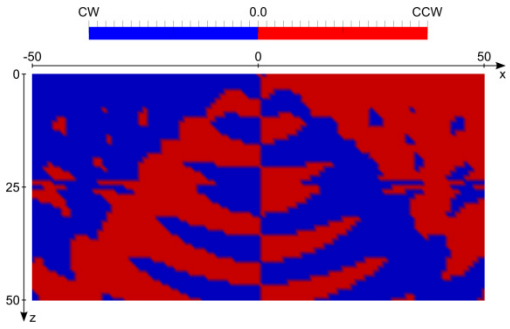

Figure 5. Rotational movement sense of the trajectories

Visualization of the phase angle

An analysis of Fig. 6, the vertical component, shows clearly two types of wave fronts. Near the surface ($z = 0$) and moving towards the edge of the domain, the wave front end to be plane. Plane wave fronts are typical of Rayleigh wave propagating in two dimensions. This picture helps corroborating that Rayleigh waves are the predominant propagating wave type near the surface and away from the energy source. The second type of wave front present an almost circular character and is typical of body waves, that is, dilatational and shear waves propagating in two dimensions [Gra91].

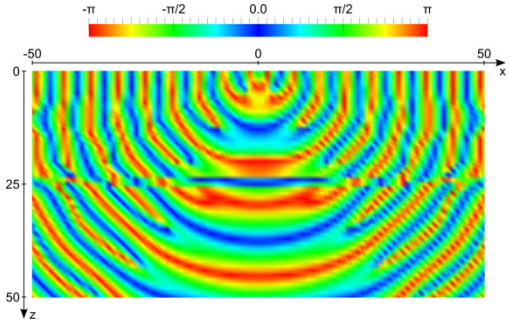

Figure 6. Phase angle of the u_z vertical component

6. CONCLUSIONS

The developed simulation software has been applied to help analyzing the wave propagation pattern resulting from the numerical solution of a very complex geomechanical problem. The numerical tools implemented in the simulation software, together with previous knowledge on the properties of wave types in solids, allowed the problem analyst to understand the various wave types that propagated through the medium and also to determine the region of their respective predominance. With the visualization environment developed, researchers can now concentrate their efforts on developing computational methods and more easily analyze the simulation results.

7. ACKNOWLEDGMENTS

Special thanks is given to Dr. Pérsio L. A. Barros for his helpful suggestions and ideas for improving the system. The first author would also like to thank CAPES/Brazil for financial support.

8. REFERENCES

[Bar99] Barros, P. L. A., and Mesquita, E. 1999. Elastodynamic Green's functions for orthotropic planestrain continua with inclined axes of symmetry. In: *International Journal of Solids and Structures*. 36, 31-32 (Nov. 1999), 4764-4788. DOI: 10.1016/S0020-7683(98)00264-9.

[Gra91] Graff, K. F. 1991. *Wave motion in elastic solids*. Dover Publications Inc., Mineola, NY, USA. ISBN: 978-0-486-66745-4.

[Lai09] Lai, W. M., Rubin, D., and Krempl, E. 2009. *Introduction to continuum mechanics*, 4th ed. Butterworth-Heinemann Ltd., Burlington, MA, USA. ISBN: 978-0-7506-8560-3.

[Mes09] Mesquita, E., Adolph, M., Carvalho, E. R., and Romanini, E. 2009. Dynamic displacement and stress solutions for viscoelastic half-spaces subjected to harmonic concentrated loads using the Radon and Fourier transforms. In: *International Journal for Numerical and Analytical Methods in Geomechanics*. 33, 18 (Dec. 2009), 1933-1952. DOI: 10.1002/nag.802.

[Raj93] Rajapakse, R. K. N. D., and Wang, Y. 1993. Green's functions for transversely isotropic elastic half space. In: *Journal of Engineering Mechanics*. 119, 9 (Sep. 1993), 1724-1746. DOI: 10.1061/(ASCE)0733-9399(1993)119:9(1724).